ACS APPLIED MATERIALS & INTERFACES

Research Article

www.acsami.org

Surface Roughening of PET Films through Blend Phase Coarsening

Ahmad Rezaei Kolahchi, Pierre J. Carreau, and Abdellah Ajji*

CREPEC, Chemical Engineering Department, Polytechnique Montreal, Montreal, Quebec, Canada

ABSTRACT: In this study, a novel method to increase the surface roughness of polyethylene terephthalate (PET) films is proposed. The mechanism of phase coarsening at the surface in extruded thin films of PET blended with low concentrations of polystyrene (PS) was investigated. A small amount of poly(hyroxyl ether) of bisphenol A (phenoxy resin, PKHH) was found to significantly increase the surface roughness due to its effect on the PS−PET interfacial tension. X-ray photoelectron spectroscopy (XPS) results indicated that in the presence of PKHH, PS droplets migrated spontaneously towards the surface of the polymer film. An increased local concentration of PS near the surface took the form of encapsulated droplets. Above the flow temperature of the blend, the local concentration of PS eventually reached a level where a co-continuous morphology occurred, resulting in the instabilities on the surface of the film. The adhesion properties of films with various roughnesses were determined using a pull-off test and found to be significantly increased, which suggested that co-continuous morphology and the coarsening process increased the adhesive properties of the film.

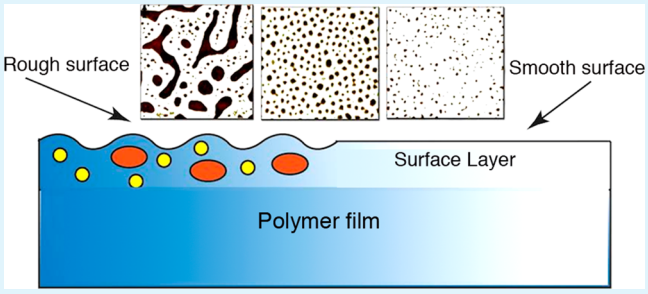

KEYWORDS: *polymer surface, surface adhesion, coarsening, PET, roughness, polymer blend*

INTRODUCTION

Despite the remarkable mechanical and physical properties of polyesters,[1−4] poor wettability and surface energy means that this class of polymers does not adhere to most materials,[5−8] precluding its use in applications such as printing and dying without previous surface treatment. Adhesion between two contacting surfaces depends on chemical bonds and mechanical interactions.[9−11] It increases in response to improved chemical and physical interactions based in part on an increase of surface energy[12−15] as well as roughness of solid surfaces.[16−21] Many different theories and models have been proposed to measure adhesion between two surfaces based on bond formation and interface interactions.[22−24] One such model proposes that adhesion is a contribution of Lifshitz−van der Waals (LW) and acid−base (AB) interactions. According to van Oss et al.,[25] such interaction can be described in quantitative terms, using the work of adhesion

$$W_a = W_a^{LW} + W_a^{AB} \quad (1)$$

where W_a is the work of adhesion and W_a^{LW} and W_a^{AB} represent the LW and AB contributions to the work of adhesion, respectively. In addition to LW and AB interactions, the work of adhesion was also shown to increase in rough surfaces because of increased surface contact.[26−28] The effect of roughness manifests itself in a number of ways. In the case of a liquid-solid interface, the liquid surface can anchor physically into the solid by penetrating into pores or by binding against concavities, a phenomenon referred to as mechanical interlocking (MI). Figure 1 shows a schematic of surface roughness and liquid anchoring in pores. Since MI increase the work of adhesion regardless of LW or AB contribution, eq 1 must be modified to account for this third factor

Figure 1. Schematic illustration of roughness and liquid anchoring on a solid surface.

$$W_a = W_a^{LW} + W_a^{AB} + W_a^{MI} \quad (2)$$

where Wa^{MI} is the MI contribution to the work of adhesion.[29−31] There are many examples of experimental work showing the effect of surface roughness on bonding area and adhesion.[32−36]

Several techniques exist for roughening polymer substrates, including but not restricted to etching the polymer surface by dissolving some components from the surface,[37−39] immersing in a reactive gas,[40] bombardment by ions,[41,42] and thermal and capillary fluctuations.[43,44] As yet, no roughening technique has been reported for use in conventional melt processing operations such as extrusion. Such a technique would be of interest because of its easy and cost-effective process.

Received: December 18, 2013
Accepted: April 14, 2014
Published: April 23, 2014

   dx.doi.org/10.1021/am4058259 | *ACS Appl. Mater. Interfaces* 2014, 6, 6415−6424

Surface roughening can be achieved during melt processing if one of the components of a polymer blend naturally migrates toward the film surface, resulting in a composition gradient across the thickness of the film. This can occur for a number of reasons such as the buoyancy forces related to the density of the polymer components or due to segregation resulting from the applied shear developed by processing.

The surface roughening in polymer blends film occurs more efficiently through forming co-continuous network morphology of two phases at the surface of the film. It is found that under flow, coalescence of droplets and the formation of a co-continuous morphology are dependent on viscoelastic parameters, whereas under static conditions, the concentration controls the morphology.[45,46] Dependent on the concentration of the phases, blends can evolve through different morphologies with their own characteristic wavelength ($\Lambda(t)$).[47] Cahn and Hilliard[48] proposed a theory describing the stage of the phase separation during which wavelengths grow in time. These wavelengths alteration can be obtained from radial average of a 2D fast Fourier transform (FFT) of the AFM topographical images or the intensity at different characteristic wavenumbers (q^*) using light scattering technique. The late stage coarsening of the phases is characterized by a power-law dependence of the domain size. The coarsening can be occur either by migration of droplets through the matrix or gradient in the capillary forces. In the former, coarsening of the domains is explained by $q^* \propto t^{1/3}$, and in the latter, it is described by $q^* \propto t^1$.

When a polymer blend with a co-continuous morphology is annealed above its flow temperature, the phase structure can become coarser to minimize the system free energy. For the case where one of the interfaces is air, the internal coarsening leads to roughening of the film at that surface. Surface roughening through phase coarsening in binary mixtures is a technique that has been widely studied, leading to rapid technological enhancements, particularly in thin polymer films.[49−54]

In this study, we investigate (1) the mechanisms for roughening polymer film surface and (2) the effect of induced roughness on polymer film surface adhesion and dyeability properties. We investigate the novel idea of roughening PET films based on the migration phenomenon that drives the system into a co-continuous morphology for a low concentration of the minor component. A method for the spontaneous migration of one desired minor component to the surface of a molten blend is applied. Then, through annealing and increasing concentration of the minor component at the surface layer, a co-continuous morphology of the PET-PS at the surface of the blend is created. The coarsening of PS droplets occurs by coalescence through which the free energy of the blend is minimized by reducing the interfacial area between the phases.

In this work, PKHH and polystyrene (PS) were used as minor phases in blends with a PET matrix. PKHH can reduce the size of PS droplets and acts as a compatibilizer for PET because of its chemical structure. It tends to act as a hydrogen bond donor, which increases its interactions with the polyester, whereas the aromatic groups of the phenoxy resin probably coordinates with those of PS. Droplet size is an important variable, because small droplets are able to migrate more quickly to the surface layer in response to shear in the extruder.

Here, annealing was used to determine the kinetic behavior of the migration of PS to the subsurface layer of the film. We investigated the kinetics of phase segregation and coarsening by 2D fast Fourier transforms (FFT) of the AFM images. To quantitatively analyze the evolution of the surface roughness, the root-mean-square surface smoothness (RMS) of the binary polymer blend films at thin surface layer and the characteristic wavenumber were introduced. The FFT transformed data exhibit a maximum intensity at a characteristic wavenumber q_{max}.

EXPERIMENTAL SECTION

Materials and Sample Preparation. For the matrix, we used a recycled PET (R-PET) supplied by Lavergne Group Inc. in thin 15 mm^2 flakes. It contains a white crystalline portion of about 5% by weight. The other polymers were: PS Styron 663 with density 1.04 g/mL and molecular weight of 300 kDa and PDI = 1.08 (supplied by Dow Chemical), PKHH phenoxy resin with M_w of 52 kDa (supplied by InChem Corp.) and deuterated PS (dPS) with M_w of 298 kDa and PDI = 1.06 (purchased from Scientific Polymer Products Inc.). For adhesion tests, a solvent borne alkyd paint (Brillant) was purchased from Timpe & Mock GmbH & co.

Before blending, PET, PS and PKHH were dried at 100, 80, and 100° C respectively in a vacuum oven for 24 h. To prepare a benchmark PET film, we extruded the dried PET using a co-rotating twin-screw extruder (CICO-TSE) manufactured by Leistritz Corp. with an L/D ratio of 40 (L = 720 mm), at a rotation speed of 100 rpm. The extruder was operated using a temperature profile of 245, 250, 255, 255, 255, 250 ° C (for the different zones from the hopper to the die). Binary polymer films (PET-PS and PET-PKHH) were prepared by direct solid mixing of PET with 5 wt % of the other component and then extruded under the conditions defined above. The ternary polymer blend film (90 wt %PET-5 wt %PKHH-5 wt %PS) was prepared using direct solid mixing of the three components before feeding into the extruder and operated under the same conditions. After each processing, the polymer films were cooled using an air-knife right after the exit of the die. Annealing was performed isothermally in a vacuum oven at temperatures in the range of 240 to 260 °C for periods ranging from 20 to 1200 s followed immediately after by quenching to 0 °C (into ice−water).

Characterization. *X-ray Photoelectron Spectroscopy (XPS).* Blends films surfaces were analyzed via XPS using a VG ESCALAB 3 MKII spectrometer. Electrons were excited using a nonmonochromatic Mg Kα x-ray source (1253.6 eV), with an experimentally determined spectral resolution of 0.7 eV and a standard measurement error of less than 0.1 eV. Pressure in the chamber was maintained at 1 × 10^{-9} Torr (1.333^{-7} Pa) and the main carbon peak was fixed to a binding energy of 284.7 eV. Relative concentrations were determined by dividing integrated intensity values by sensitivity factors taken from the Wagner table.[55] An area of approximately 5 mm in diameter of sample surface was analyzed. Survey scans (0−1100 eV) and narrow scans (high resolution) of the C 1s and O 1s regions were obtained. Peak fitting of the C 1s and O 1s core levels was carried out using the Avantage V 4.12 software. Consequently, the O/C atom ratio was estimated from the relative peak intensities of the O 1s and C 1s spectra.

Surface Morphology. The surface morphology and topography of the films was studied via scanning electron microscopy (SEM) and atomic force microscopy (AFM). SEM observations were conducted using a Hitachi S-4700 operated at 10 kV and the samples were coated prior to the test with gold−palladium alloy by plasma sputtering for 15 s. AFM imaging was performed on a Dimension 3100 Nanoscope V controller from Digital Instruments Inc. (Santa Barbara, CA) in the tapping mode. ACTA Cantilevers from Applied Nano Inc. with a spring constant of 42 N/m, resonance frequency of 300-400 kHz and medium oscillation damping with the set point of 75% amplitude were used. Samples were ultra-microtomed to observe morphology of the cross-section, using a diamond knife at room temperature.

Depth Profiling. Depth profiling was used to determine the concentration of the components of a blend film as a function of depth when the information on the wetting properties of multicomponent polymer mixtures was required. It is a useful technique to analyze the

segregation of the components in an unstable blend if this segregation corresponds to a wetting layer. By this technique the elements below the surface region, layer by layer, are determined in the forward direction from a depth ranging from 0 to 5000 Å. One of the direct depth profiling method is MeV ion beam scattering. A beam of ions produced by an accelerator is incident on the sample. The ions are scattered from the surface and the emitted particles due to fragments from collision or nuclear reaction are detected.

In this study, FRES was performed on a model 5SDH Pelletron tandem accelerator (National Electrostatic Corporation, WI), interfaced with a scattering chamber. The technique has been described elsewhere.[56] Briefly, 1.51 MeV 4He+ ions impinge on a target at an angle 78° with respect to the normal of the sample. The H and D atoms in the target surface are forward scattered and detected. The SIMNRA analysis program 30 version 5.02, was used to analyze the spectra.[57]

Adhesion Test. One of the aims of this work is to investigate the effect of roughness created through polymer blending on the adhesion of paint on the surface of the polymer. In this investigation, pull-off test can be used to measure the adhesion strength between coating layers. The pull-off adhesion test is a quantitative technique in which a metal surface called a dolly is bonded to the surface in question using an epoxy resin. The pull-off tests were performed with an automatic PosiTest Pull-off Adhesion Tester (PosiTest At-A from DeFelsko Corp., USA) in accordance with ASTM D4541 and ISO 4624 under constant stress and fixed rate of loading of 1 MPa/s. A schematic of this test method is shown in Figure 2. In this method, an aluminum

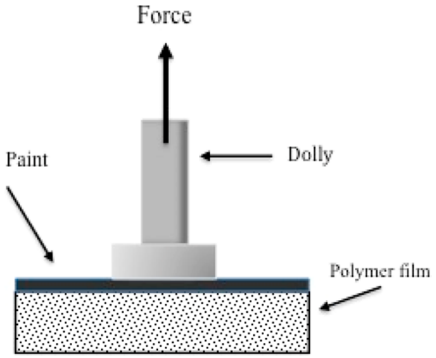

Figure 2. Schematic image of pull-off adhesion test.

made dolly is glued to the specimen whose adhesion is to be tested, and a tensile load is applied until failure. The tensile force required breaking the bond between the dolly and the surface is then calculated. We used aluminum dollies with a diameter of 10 and 25 mm and a two-component epoxy-based adhesive (Araldite 2011) to glue the dollies to the test specimens. This tester exerts tensile loads generated by an electrical hydraulic pump. In this experiment the PosiTest pull-off adhesion tester was used to evaluate the adhesion of alkyd paint to the prepared film surfaces.

Measurement of Interfacial Tension. Films of PET of 0.5 mm thickness were pressed between two metal plates on a Carver laboratory press at 250 °C. The PS and PKHH fibers were prepared manually. The fiber diameters ranged from 40 to 100 μm. The fibers were cut to 25 mm lengths and annealed at 60 °C for about 24 h in a vacuum oven to remove any residual stress. The breaking thread technique was used to measure the interfacial tension between PET and PKHH and PS at 200 and 240 °C. In the breaking thread method, the interfacial tension between two polymers can be measured by following the initial stages of breakup of a fiber of one of the polymers sandwiched in the other one to form small droplets as a function of time.[45] A Mettler hot-stage model FP 82 HT connected to a FP 90 central processor and to a Nikon transmission optical microscope was used. The tests were conducted for two PET films and a thread of PS or PKHH was sandwiched between the PET films mounted on glass sides and then placed under the microscope of a hot stage. The temperature of the hot stage was raised to the desired temperatures and periodic digital images from the microscope were captured. At least 15 series of measurements were carried out. Details about the measurement and calculations of interfacial tension were reported elsewhere.[58,59] Figure 3 shows sinusoidal distortion on the PS thread embedded in the PET matrix.

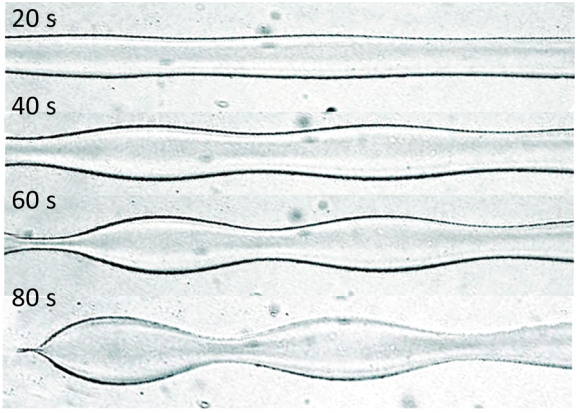

Figure 3. Sinusoidal distortions on the PS thread with diameter 55 μm, embedded in the PET matrix. The measurement was performed at 240 °C; the times at which subsequent photographs were taken are t = 20 , 40, 60, 80 s.

RESULTS AND DISCUSSION

XPS Analysis. XPS measurements were performed with 0.1 eV steps on the film samples to determine the relative content of carbon and oxygen atoms on their surfaces. The C 1s spectrum has been fitted with three distinctly resolved peaks attributed to carbon atoms located in benzene rings (C marked with I in Figure 4a), carbon bonded to oxygen (C marked with II in Figure 4a) and ester atoms group (C marked with III in Figure 4a) identified in the chemical structure of PET shown in Figure 4. The oxygen (O 1s) spectrum was also fitted with two contributions: carbonyl oxygen (O marked with I in Figure 4-a) and singly bonded oxygen (O marked with II in Figure 4a). The XPS spectra of C 1s and O 1s for neat PET film surface, polymer blend of PET-5 wt %PS-5 wt %PKHH and the blend of PET-5 wt %PS and also the XPS spectra of O 1s for the samples are observed in Figure 4b from 1 to 6 respectively. Relative abundance of carbon and oxygen atoms and the types of bonds they form were determined from the area of peaks corresponding to those identified previously. Table 1 shows the relative contents of the different types of oxygen and carbon for the neat PET, the binary (PET−PS) and the ternary blend films. The CI peak at a binding energy of 284.7 eV, which corresponds to carbon atoms in phenyl rings (C−H and C−C) for the PET-5 wt %PS-5 wt %PKHH, changes significantly compared to the same spectrum for the neat PET film surface whereas for the binary blend, it is almost the same as for the neat one. Also, CII and CIII peaks remarkably decrease for the ternary blend while OI/OII ratio remains almost constant for the all samples. Additionally, the total concentration of oxygen molecules decreases from 27.6 for neat PET to 15.9% for PET-PS-PKHH blend, while there is no significant change for the binary one compare to neat PET film. Since PKHH chains contain two −C−O− and one −OH functional groups with almost 17% O/C ratio, the changes indicate the presence of more PS at the top layer of few nanometers (analytical depth of XPS) of the surface of the film. The results indicate that, at a

dx.doi.org/10.1021/am4058259 | ACS Appl. Mater. Interfaces 2014, 6, 6415−6424

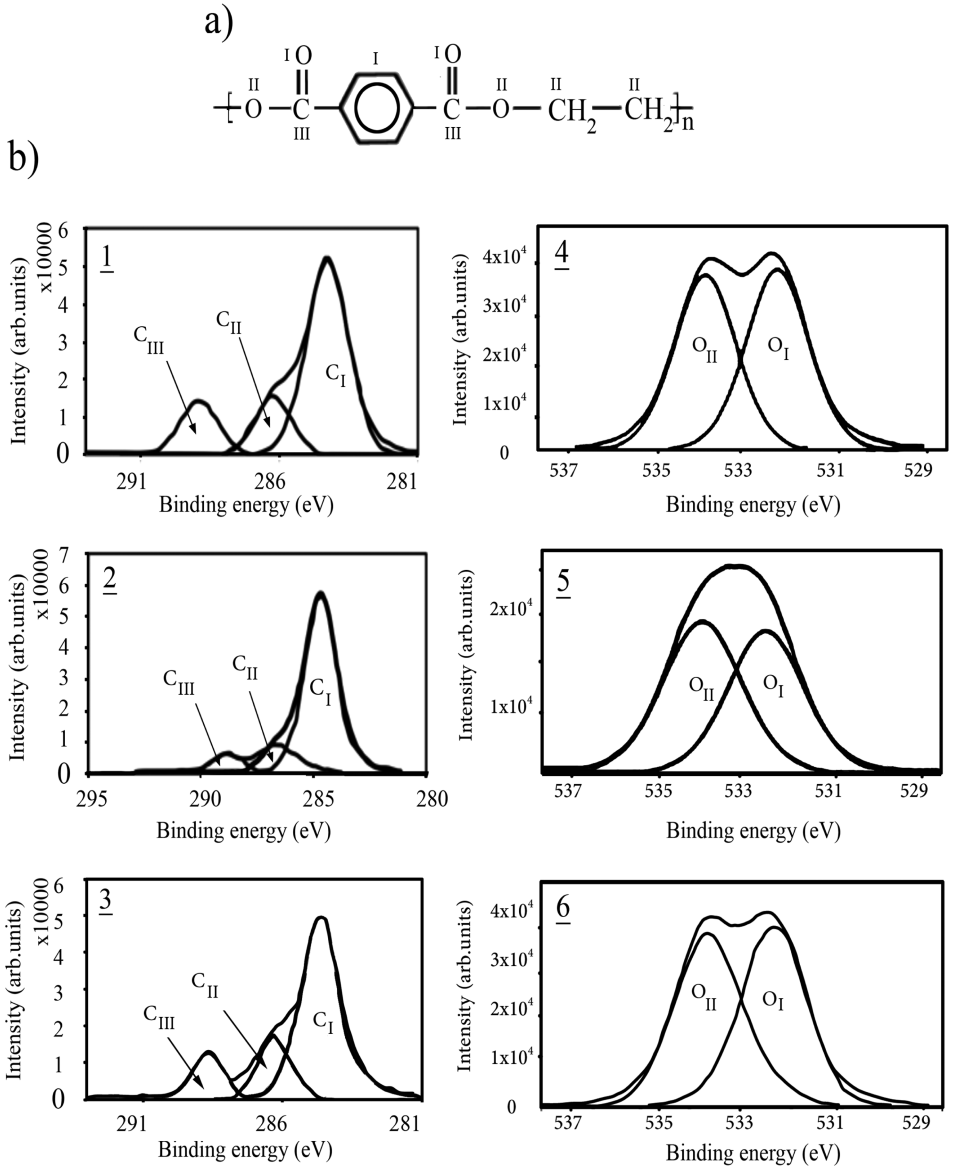

Figure 4. (a) Chemical structure of PET. (b) High-resolution XPS spectra of: 1 C 1s PET, 2 C 1s PET-5 wt %PS-5 wt %PKHH, 3 C 1s PET-5 wt % PS, 4 O 1s PET, 5 O 1s PET-5 wt %PS-5 wt %PKHH, 6 O 1s PET-5 wt %PS.

Table 1. High-Resolution XPS Spectra of PET and PET-5 wt %PS-5 wt %PKHH Film Surfaces

		C 1s			O 1s			
		CI	CII	CIII	OI	OII	C	O
PET	peak BE (eV)	284.7	286.4	288.7	531.7	533.1	72	27.6
	at %	47.7	12.9	11.8	14	13.6		
PET-5 wt %PS-5 wt %PKHH	peak BE (eV)	284.7	286.6	288.7	531.9	533.3	84.1	15.9
	at. %	68.5	8.7	6.9	8.1	7.8		
PET-5 wt %PS	peak BE (eV)	284.7	286.6	288.6	531.7	533.3	73.4	26.6
	at %	48.3	13.7	11.4	13.5	13.1		

given concentration of the minor phases, the surface layer of the film is enriched with PS, whereas PKHH is less apparent in this layer. No significant change in the surface concentration of carbon and oxygen of the PET−PS film indicates that there is no remarkable movement of PS molecules to the surface of the film. The solubility parameter of the phenoxy resin implies more compatibility with polar materials such as polyesters and nylons, but less compatibility with acrylics, olefins, and vinyls. Measurements of the interfacial tension between PKHH and PET (approximately 0.4 ± 0.2 mN/m) and between PET and PS (approximately 4.2 ± 0.8) mN/m) explain the tendency of PKHH to mix well with PET, and the tendency of PS to migrate from the bulk of the polymer to the surface layer during the extrusion process. It should be noted that the surface free energy of PET and PS are 44.6 and 40.7 mN/m, respectively, at 20 °C.[60,61] Therefore, it can be concluded from XPS results that PS is preferentially present at the surface layer of the polymer blend.

dx.doi.org/10.1021/am4058259 | ACS Appl. Mater. Interfaces 2014, 6, 6415−6424

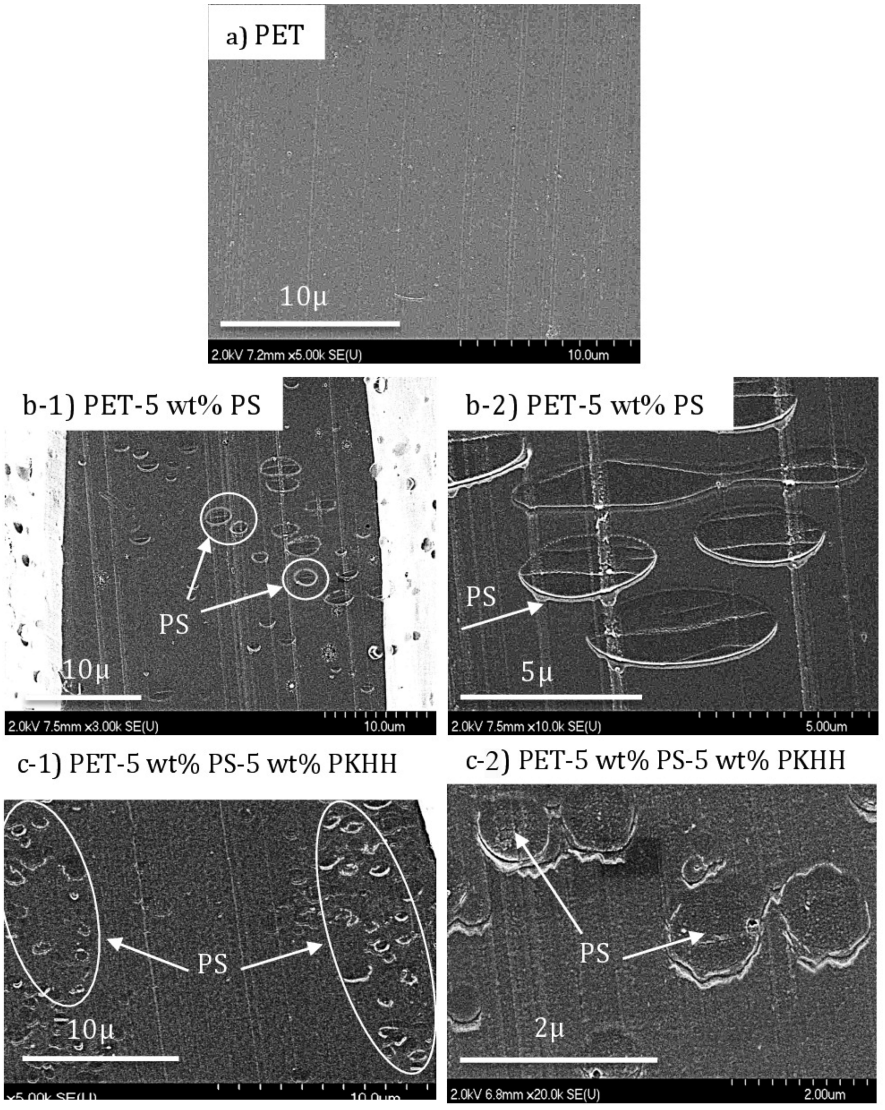

Figure 5. SEM images from (a) PET film surface. (b-1) Cross-section of PET-5 wt %PS. (b-2) PET-5 wt %PS film surface. (c-1) Cross-section of PET-5 wt %PS-5 wt %PKHH films. (c-2) PET-5 wt %PS-5 wt %PKHH film surface.

SEM Results. Figure 5 exhibits SEM micrographs of the cross-section (b-1 and c-1) and surface (a, b-2, and c-2) of a PET film, a film of a binary blend of PET−PS and a film of a ternary polymer blend of PET-PS-PKHH, all for several magnifications. Because of the very low interfacial tension between PET and PKHH, they are almost miscible and PKHH cannot be observed as droplet in PET matrix. Therefore, the images of PET films containing 5 wt %PS show a uniform distribution of PS droplets in the bulk of the film. Those presented in Figure 5b-1 show PS droplets well distributed regardless of the depth. Images of Figure 5b-2 present the size and shape of the PS droplets. They are oval-like droplets with a diameter of 4 μm on average with smooth interfaces. In the SEM images of the ternary polymer blend, the PS droplets are completely different in terms of distribution, size and shape. As can be observed from the Figure 5c-1 image, the distribution of the PS droplets within the film is not as homogenous as in the PET-PS film. Droplets of PS are abundant near the surfaces of the film and scarce in the bulk. Further, images of Figure 5c-2 show that PS droplet size has decreased significantly to an average of less than 2 μm in diameter in response to the addition of PKHH to the system. Another observation from these micrographs is that the addition of PKHH has resulted in a rougher interface between PET and PS.

Depth Profiling and AFM Results. Segregation in polymer blends can be observed by the variation of three parameters, namely temperature, composition and molecular weight. In this work, the temperature was modulated (annealing), whereas the other variables were kept constant in order to determine an ideal processing condition for extrusion. Therefore, we annealed the blend films at a controlled temperatures and characterized them using FRES technique.

FRES depth profiling was used to characterize the polymer/air interface of the ternary polymer blend. Figure 6 presents the FRES profile along with AFM images of the PET-dPS−PKHH film for different annealing times at 250 °C. Deuterated polystyrene (dPS) with the almost same characteristics of the PS was used in the blend to evaluate by depth profile technique whether the polystyrene chains change their locations at the surface layer during annealing. Deuterium and hydrogen from the film are elastically scattered and detected by a detector located at −75°. The surface depth resolution has a full-width half-maximum value of 800 A. Figure 6a reports the FRES

dx.doi.org/10.1021/am4058259 | ACS Appl. Mater. Interfaces 2014, 6, 6415−6424

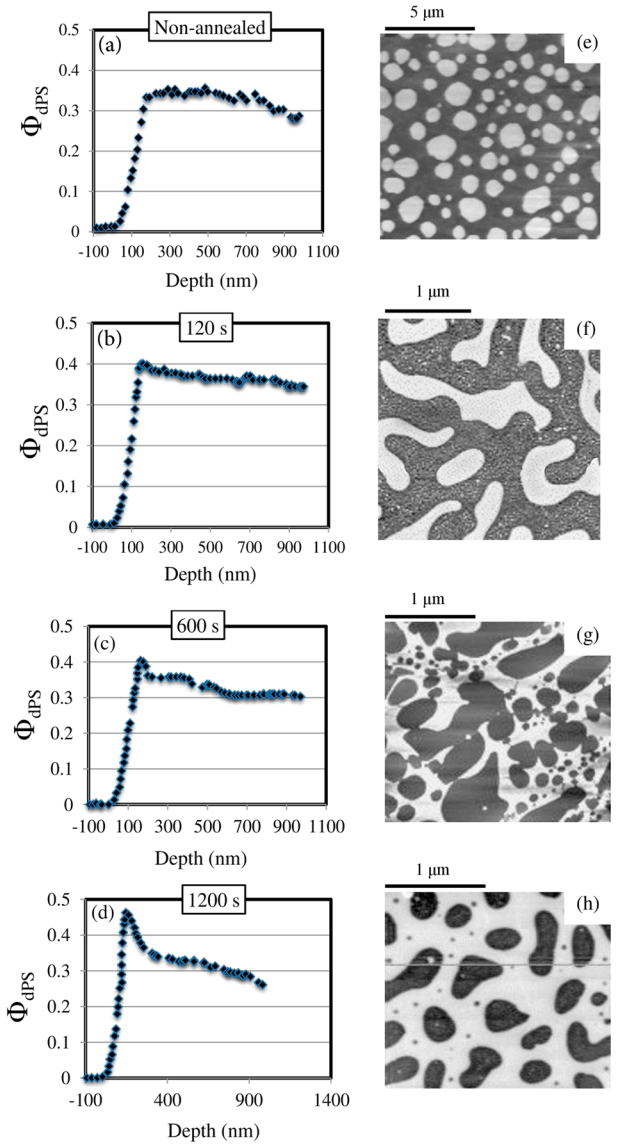

Figure 6. Volume fractions of dPS from FRES depth profiles of PET-5 wt %dPS-5 wt %PKHH film surface for (a) non-annealed sample. and annealed samples at 250 °C for (b) 120, (c) 600, and (d) 1200 s; and AFM phase images of PET-5 wt %dPS-5 wt %PKHH film surfaces for (e) non-annealed sample and annealed samples at 250 °C for (f) 120, (g) 600, and (h) 1200 s. Scan sizes are 2.5 μm × 2.5 μm (dark region is PET and bright region is PS).

profile for the PET-dPS-PKHH film without annealing. The graph indicates that dPS is located at the surface layer of the polymer film surface, which is consistent with the results of XPS. Although dPS makes up only 5 wt % of the blend, the volume fraction of dPS at the layer close to the surface is about 35%. This indicates that most of the dPS droplets have segregated to the polymer/air interface during extrusion and film solidification. Annealing resulted in migration of more dPS molecules from the bulk to the subsurface layer. A comparison between Figure 6a and Figure 6b–d indicates that the concentration of dPS at the surface layer increases with annealing time. After 120 s annealing, the rate of migration is higher than what was initially expected based on the lower surface tension of dPS compared to PET. The average movement of PS molecules can be estimated using the Einstein equation ($l^2 = 2Dt$)[62] where l^2 is the mean free quadratic displacement in one direction, D is the diffusion coefficient, and t is the diffusion time. The typical diffusion coefficient of PS is $D = 2.8 \pm 0.07 \times 10^{-11}$ (cm^2/s),[62] so it was estimated that in the course of 1 s, the average displacement of the PS molecules is 10 nm. Because the thickness of the prepared film is around 30 μm, the migration of PS molecules from the middle of film to the surface layer would take around 25 min if only the diffusion mechanism is involved. Therefore, the migration cannot be described only by the diffusion and surface tension difference, while under this driving force more time (not in the scale of seconds) is needed for the migration of a component to the surface. Consequently, other factors such as density differences and viscosity ratio must also influence the migration of dPS droplets.

The right column of Figure 6e–h shows the topography of dPS-rich layer at the surface. Phase imaging in tapping mode was used to obtain contrast based on surface hardness. The dark zones are associated with PET phase, whereas the brighter ones with PS. There is a sharp contrast between the PET and PS phases. It is suggested that phase contrast images of the samples are related to surface stiffness variations associated with changes in the elastic modulus. However, the enhancement of the concentration of polystyrene in AFM images is correlated with the results from XPS and FRES. The PS phase could also be distinguished because of its higher elastic modulus (5.12 GPa) compared to the PET (3.05 GPa).

According to the AFM images, the surface topography changes with time to exhibit a co-continuous surface pattern in the PET film. Figure 6f shows the surface after 120 s. The images show that phase coarsening starts to develop gradually with segregation of dPS in the blend. Thus, there is a dPS-rich unstable layer (about 500 nm from the top) and a PET-rich bulk region. With further annealing, we observe an increasing concentration of dPS in the surface layer. By combining the depth profile and the surface topography of the films, the roughness evolution can be described in terms of phase coarsening of co-continuous morphology occurring on the polymer surface.

To conclude, segregated dPS droplets are present near the surface layer before annealing. Annealing at 250 °C for 120 s increases the polymer chains' mobility along with the dPS concentration in the subsurface layer, followed by the formation of a co-continuous structure. When annealing for 500 or 1200 s, the co-continuous structure coarsens, along with phase inversion.

Phase Coarsening Kinetics. The phase coarsening kinetics was investigated by analyzing the evolution of the surface roughness correlation length $\lambda(t) = 2\pi/q_{max(t)}$ on the polymer film surface, where $q_{max(t)}$ is a characteristic wavenumber corresponding to peak maximum. $q_{max(t)}$ can be obtained from the fast-Fourier transform (FFT) of AFM images. The two-dimensional FFT spectrum exhibits a maximum intensity at a characteristic wavenumber (q_{max}). The first stage of phase coarsening identified in this process is consistent with the linearized theory developed by Cahn and Hilliard.[48] Later in the evolution of the coarsening, a different trend is identified, wherein peak wavenumber shows a power law dependence on time: $q(t) \approx t^{-n}$. Several articles have focused on this power-law behavior. Geoghegan has reviewed the phase behavior of polymer blend on polymer surface in detail.[63]

The analysis of AFM images by 2D FFT over a square section of 512 × 512 pixels was performed. The intensity as a function of wavenumber for the PET–PS-PKHH film was

obtained from the circular average of the 2D FFT from AFM images. The results achieved after annealing to find q_{max} values and phase evolution kinetics. The right inset in Figure 7 shows

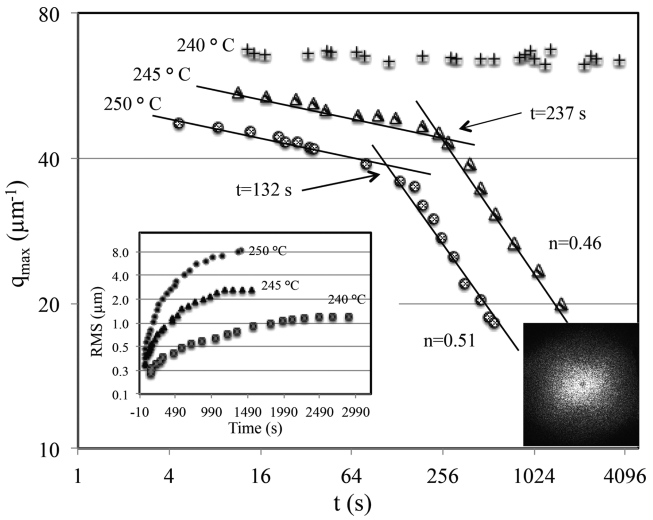

Figure 7. Characteristic wavenumber versus annealing time for the PET-PS-PKHH blend at three different temperatures (240, 245, and 250 °C). The left inset shows RMS surface roughness as a function of annealing time at different temperatures (240, 245, and 250 °C) and the right inset shows 2d FFT image of PET-5 wt %PS-5 wt %PKHH film.

2D FFT image for this sample. The left inset in Figure 7 shows the PET-PS-PKHH film surface roughness as a function of time at different annealing temperatures. The RMS roughness increases with time for all samples. For samples annealed at 250 and 245 °C, the RMS roughness initially increases sharply, whereas at 240 °C, a plateau is reached after a slight increase. The q_{max} value as a function of time is plotted in Figure 7 at different annealing temperatures on logarithmic scales. For the sample annealed at 240 °C, q_{max} is constant over the entire experimental period, suggesting that coalescence did not occur at this temperature and the surface roughness at the beginning of the annealing (shown in left inset) could be due to the thermal fluctuations. For the samples annealed at 245 and 250 °C, q_{max} displays two distinct evolution stages. They are represented by two distinct linear trends in the plot of q_{max} as a function of time. These two trends intersect after 132 s of annealing at 250 °C and after 237 s of annealing at 245 °C. The evolution of the characteristic wavenumber can be well approximated by a power-law dependence. As previously mentioned, each sample displayed two types of phases with different trends. The power-law exponents best representing these trends are 0.05 and 0.46 for the sample annealed at 245 °C and 0.06 and 0.51 for the sample annealed at 250 °C, in order of occurrence. These trends suggest that the characteristic wavenumber is initially independent of annealing time, consistent with Cahn's linearized theory for the early stage of spinodal decomposition.[48] Ultimately, the characteristic wavenumber does change according to a power-law behavior, a phenomenon frequently observed during phase coarsening of polymer blends.

In prior work, kinetic models have been proposed for surface phase coarsening for a range of systems. Sung[64] modeled the coarsening kinetics of a PS/polybutadiene (PB) using two power-law trends, with the initial phase best modeled by the exponent 1/3 and the subsequent phase modeled by an exponent of 1. Phase coarsening and the phase behavior of polymer blends are much more complicated in thin films than in thick ones because of the significant effect of the substrate surface properties (the solid surface on which the thin film is located on) and film thickness. For example, the concentration gradient is a strong function of thickness.[65−68]

In regards to the PET-PS system, annealing above the flow temperature allows droplets of the minor phase to migrate to the surface. This migration process is probably the first phase identified. This phase is not as visible with regard to a characteristic wavenumber because diffusion of this minor phase would be relatively slow and the subsurface concentration would not yet be sufficient for formation of co-continuous morphology and starting the phase coarsening. Once the subsurface concentration of the minor phase reaches the critical concentration for phase coarsening, the co-continuous structure occurs. The effect of temperature on diffusion is clear from the fact that migration occurs faster for the sample annealed at 250 °C than for the one annealed at 245 °C. This indicates that the critical subsurface minor phase concentration was reached more quickly for the former than for the latter. The model of phase coarsening derived for annealed films suggests that if the residence time of an extruded polymer film is sufficiently long (more than 3 min) in the sheet die at 250 °C, the film would be roughened to a similar degree as an annealed one of the same composition.

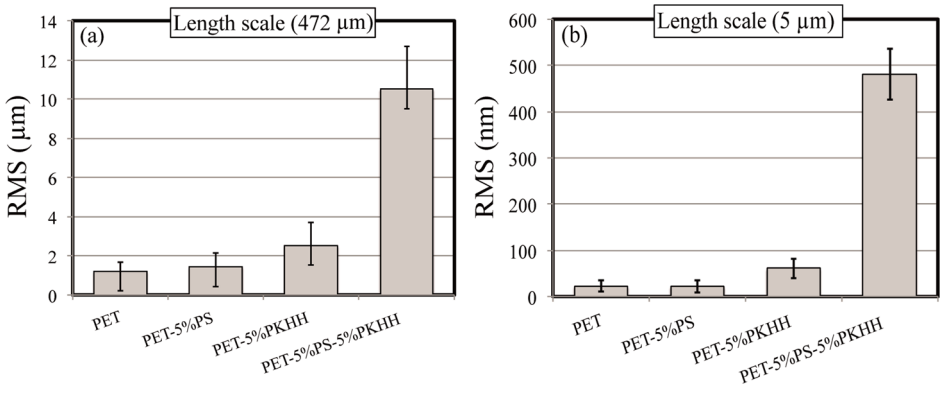

Figure 8. RMS surface roughness for the neat PET, PET-5 wt %PS, PET-5 wt % PKHH, and PET-5 wt %PS-5 wt %PKHH films surfaces in (a) 472 μm length scale and (b) 5 μm length scale.

dx.doi.org/10.1021/am4058259 | ACS Appl. Mater. Interfaces 2014, 6, 6415−6424

Surface Roughness. A profilometer was utilized to determine the average roughness of a 50 mmx50 mm square sample surface. The technique allowed comparison of the surface topography of neat PET film with the topographies of aforementioned binary and ternary blends films. Average surface roughness was treated on two different length scales to represent the different scales of roughness. Average roughness for the two length scales, namely 472 and 5 μm, are shown in Figures 8 a and b, respectively. The ternary polymer blend is significantly rougher than the other blends, with an RMS roughness of 481 nm and 10.5 μm for the 5 and 472 μm length scale measurements, respectively. These results can, in conjunction with SEM images, confirm the effect of PKHH on the surface roughening of the PET film for the two scale levels.

Adhesion Test. The adhesion strength between the prepared films of PET, PET-5 wt %PS, PET-5 wt %PKHH and PET-5 wt %PS-5 wt %PKHH as measured by the pull-off test are reported in Figure 9. As expected, the surface of the ternary polymer blend adhered more strongly to the paint than the surface of films produced from the neat PET or from the binary blends. 7.8 MPa is the required force to separate the paint from the surface of PET-PS-PKHH film, whereas applying 4.6 MPa was enough for the neat PET film at room temperature. This observation is consistent with the results of profilometery of the same films, which showed in the previous section that the ternary polymer blend film is rougher than those produced from the binary blends or neat PET.

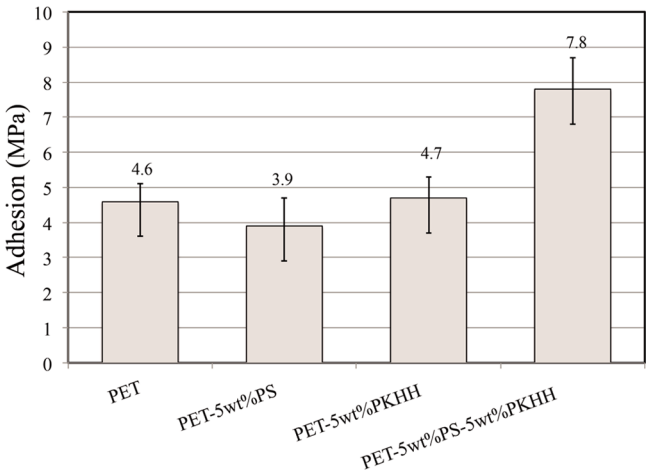

Figure 9. Adhesion test results on the surface of PET, PET-5 wt %PS, PET-5 wt %PKHH, and PET-5 wt %PS-5 wt %PKHH film.

CONCLUSION

In conclusion, this study proposed a scenario for surface roughening of PET films through melt blending. In this particular work, 5 wt %PS and 5 wt %PKHH phenoxy resin were blended with PET in a twin-screw extruder. PS droplets were initially well distributed within the bulk PET. The size of these droplets was reduced by the presence of PKHH. The reduction in droplet size permitted more and faster migration of the droplets through the continuous phase, allowing segregation to the surface layer in response to the shear forces applied by the extruder. Despite the relatively low concentration of PS, migration of these droplets to the surface of the polymer resulted in a locally unstable concentration of PS, leading to phase coarsening.

XPS results confirmed a chemical modification of the PET film surface in response to the addition of PS and PKHH in the concentrations. Use of FRES demonstrated the high concentration of PS at the film surface. Also, a co-continuous pattern due to the high concentration of the PS molecules at the surface and their coalescence was observed in AFM images.

It was also found that the critical surface phase coarsening temperature for PET−PS polymer blend was around 245 °C. When the surface concentration of PS reached an unstable level, the characteristic wavenumber followed a power-law trend best fitted by an exponent of 0.42. The transition between PET and PS phases occurred after132 s for the sample annealed at 250 °C.

Finally, pull-off tests indicated that the surface of ternary polymer blend of PET-PS-PKHH film had better adhesive properties (7.8 MPa) than surfaces of the binaries (PET-PS (4.6 MPa), PET-PKHH (4.8 MPa)) and the neat PET films (3.9 MPa).

AUTHOR INFORMATION

Corresponding Author

*E-mail: abdellah.ajji@polymtl.ca.

Notes

The authors declare no competing financial interest.

ACKNOWLEDGMENTS

The authors thank A. Yaghoobi, F. Tofan, and D. Davidescu for helpful support and discussions. Financial support from NSERC (Natural Science and Engineering Research Council of Canada) and Lavergne Group Inc. are gratefully acknowledged.

REFERENCES

(1) Du, J. Z. Synthesis and Characterization of Photo-Cross-Linked Hydrogels Based on Biodegradable Polyphosphoesters and Poly(ethylene glycol) Copolymers. *Biomacromolecules* **2007**, *8*, 3375−3381.
(2) Lemmouchi, Y.; Schacht, E. Preparation and in Vitro Evaluation of Biodegradable Poly(∈-Caprolactone-Co-D,L Lactide)(X-Y) Devices Containing Trypanocidal Drugs. *J. Controlled Release* **1997**, *45*, 227−233.
(3) Park, J. H. Polymeric Nanomedicine for Cancer Therapy. *Prog. Polym. Sci.* **2008**, *33*, 113−137.
(4) Wu, J.; Chu, C. C. Block Copolymer of Poly(Ester Amide) and Polyesters: Synthesis, Characterization, and in Vitro Cellular Response. *Acta Biomater.* **2012**, *8*, 4314−4323.
(5) Bax, D. V. Directed Cell Attachment By Tropoelastin on Masked Plasma Immersion Ion Implantation Treated PTFE. *Biomaterials* **2011**, *32*, 6710−6718.
(6) Chan, C. M.; Ko, T. M.; Hiraoka, H. Polymer Surface Modification by Plasmas and Photons. *Surf. Sci. Rep* **1996**, *24*, 1−54.
(7) Chu, P. K. Plasma-surface Modification of Biomaterials. *Mater. Sci. Eng.* **2002**, *36*, 143−206.
(8) Dargaville, T. R. High Energy Radiation Grafting of Fluoropolymers. *Prog. Polym. Sci.* **2003**, *28*, 1355−1376.
(9) Awaja, F. Adhesion of Polymers. *Prog. Polym. Sci.* **2009**, *34*, 948−968.
(10) Dubois, L. H.; Zegarski, B. R. High Energy Radiation Grafting of Fluoropolymers. *J. Phys. Chem.* **1993**, *97*, 1665−1670.
(11) Sheth, S. R.; Efremova, N.; Leckband, B. R. Interactions of Poly(ethylene oxide) Brushes with Chemically Selective Surfaces. *J. Phys. Chem. B* **2000**, *104*, 7652−7662.
(12) Patel, S. S.; Tirrell, M. Measurement of Forces Between Surfaces in Polymer Fluids. *Annu. Rev. Phys. Chem.* **1989**, *40*, 597−635.

(13) Semenov, A.N. Interaction between Two Adsorbing Plates: The Effect of Polymer Chain Ends. *Macromolecules* **1997**, *30*, 1479−1489.
(14) Katano, Y.; Tomono, H.; Nakajima, T. Surface Property of Polymer Films with Fluoroalkyl Side Chains. *Macromolecules* **1994**, *27*, 2342−2344.
(15) Owens, D. K.; Wendt, R. C. Estimation of the Surface Free Energy of Polymers. *J. Appl. Polym. Sci.* **1969**, *13*, 1741−1747.
(16) Gent, A. N.; Lin, C. W. Model Studies of the Effect of Surface Roughness and Mechanical Interlocking on Adhesion. *J. Adhes.* **1990**, *32*, 113−125.
(17) Ramanathan, T. Functionalized Graphene Sheets for Polymer Nanocomposites. *Nat. Nanotechnol.* **2008**, *3*, 327−331.
(18) Anastasiadis, S. H.; Hatzikiriakos, S. G. The Work of Adhesion of Polymer/Wall Interfaces and Its Association with the Onset of Wall Slip. *J. Rheol.* **1998**, *42*, 795−812.
(19) Paiva, A. Study of the Surface Adhesion of Pressure-Sensitive Adhesives by Atomic Force Microscopy and Spherical Indenter Tests. *Macromolecules* **2000**, *33*, 1878−1881.
(20) Ridgway, C. J.; Gane, P. A. C. Ink-Coating Adhesion: The Importance of Pore Size and Pigment Surface Chemistry. *J. Dispersion Sci. Technol.* **2005**, *25*, 469−480.
(21) Rezaei Kolahchi, A.; Ajji, A.; Carreau, P. J. Enhancing Hydrophilicity of Polyethylene Terephthalate Surface through Melt Blending. *Polym. Eng. Sci.* **2014**, *10*, 2390−2499.
(22) Baldan, A. Adhesively-Bonded Joints and Repairs in Metallic Alloys, Polymers and Composite Materials: Adhesives, Adhesion Theories and Surface Pretreatment. *J. Mater. Sci.* **2004**, *39*, 1−49.
(23) Buckton, G.; Chandaria, B. Consideration of Adhesion to Modified Container Walls, by Use of Surface Energy and Polarity Data, and Lewis Acid-Lewis Base Interactions. *Int. J. Pharm.* **1993**, *94*, 223−229.
(24) McCafferty, E. Acid-Base Effects in Polymer Adhesion at Metal Surfaces. *J. Adhes. Sci. Technol.* **2002**, *16*, 239−255.
(25) Van Oss, C. J.; Good, R. J.; Chaudhury, M. K. Additive and Nonadditive Surface Tension Components and the Interpretation of Contact Angles. *Langmuir* **1988**, *4*, 884−891.
(26) Miwa, M. Effects of the Surface Roughness on Sliding Angles of Water Droplets on Superhydrophobic Surfaces. *Langmuir* **2000**, *16*, 5754−5760.
(27) Price, R. L. Nanometer Surface Roughness Increases Select Osteoblast Adhesion on Carbon Nanofiber Compacts. *J. Biomed. Mater. Res., Part A* **2004**, *70A*, 129−138.
(28) Wenzel, R. N. Surface Roughness and Contact Angle. *J. Phys. Colloid Chem.* **1948**, *53*, 1466−1467.
(29) Gent, A. N.; Lin, C. W. Model Studies of the Effect of Surface Roughness and Mechanical Interlocking on Adhesion. *J. Adhes.* **1990**, *32*, 113−125.
(30) Kim, W. S. Evaluation of Mechanical Interlock Effect on Adhesion Strength of Polymer-Metal Interfaces Using Micro-Patterned Surface Topography. *Int. J. Adhes. Adhes.* **2010**, *30*, 408−417.
(31) Packham, D. E. Work of Adhesion: Contact Angles and Contact Mechanics. *Int. J. Adhes. Adhes.* **1996**, *16*, 121−128.
(32) Davis, C. S.; Crosby, A. J. Mechanics of Wrinkled Surface Adhesion. *Soft Matter* **2011**, *7*, 5373−5381.
(33) Fuller, K. Effect of Surface Roughness on the Adhesion of Elastomers to Hard Surfaces. *Mater. Sci. Forum.* **2010**, *662*, 39−51.
(34) Maugis, D. On the Contact and Adhesion of Rough Surfaces. *J. Adhes. Sci. Technol.* **1996**, *10*, 161−175.
(35) Mazzitelli, C. Surface Roughness Analysis of Fiber Post Conditioning Processes. *J. Dent. Res.* **2008**, *87*, 186−190.
(36) Peng, Z. L.; Chen, S. H. Effects of Surface Roughness and Film Thickness on the Adhesion of a Bioinspired Nanofilm. *Phys. Rev. E: Stat., Nonlinear, Soft Matter Phys.* **2011**, *83*, 051915.
(37) Fu, X.; He, X. Fabrication of Super-hydrophobic Surfaces on Aluminum Alloy Substrates. *Applied Surface Science* **2008**, *255*, 1776−1781.
(38) Qian, B.; Shen, Z. Fabrication of Superhydrophobic Surfaces by Dislocation-Selective Chemical Etching on Aluminum, Copper, and Zinc Substrates. *Langmuir* **2005**, *21*, 9007−9009.
(39) Chun, Y. W. The Role of Polymer Nanosurface Roughness and Submicron Pores in Improving Bladder Urothelial Cell Density and Inhibiting Calcium Oxalate Stone Formation. *Nanotechnology* **2009**, *20*, 85104.
(40) Lee, H. U. Surface Modification of and Selective Protein Attachment to a Flexible Microarray Pattern Using Atmospheric Plasma with a Reactive Gas. *Acta Biomater.* **2010**, *6*, 519−525.
(41) Dai, W. Ion-Beam Induced Surface Roughening of Poly-(methyl methacrylate) (PMMA) Tuned by a Mixture of Ar and O2 Ions. *Plasma Process. Polym.* **2012**, *9*, 975−983.
(42) Ting, Y. H. Surface Roughening of Polystyrene and Poly(methyl methacrylate) in Ar/O2 Plasma Etching. *Polymers* **2010**, *2*, 649−663.
(43) Vrij, A.; Overbeek, J. T. G. Rupture of Thin Liquid Films Due to Spontaneous Fluctuations in Thickness. *J. Am. Chem. Soc.* **1968**, *90*, 3074−3078.
(44) Wyart, F. B.; Daillant, J. Drying of Solids Wetted by Thin Liquid Films. *Can. J. Phys.* **1990**, *68*, 1084−1088.
(45) Andradi, L. N.; Hellmann, G. P. Morphologies of Mechanically Mixed Amorphous Blends Before and after Annealing. *Polym. Eng. Sci.* **1995**, *35*, 693−702.
(46) Utracki, L. A. On the Viscosity-Concentration Dependence of Immiscible Polymer Blends. *J. Rheol.* **1991**, *35*, 1615−1637.
(47) Scholten, E.; Sagis, L. M. C.; Van der Linden, E. Bending Rigidity of Interfaces in Aqueous Phase-Separated Biopolymer Mixtures. *Macromolecules* **2005**, *38*, 3515−3518.
(48) Cahn, J. W.; Hilliard, J. E. Free Energy of a Nonuniform System. I. Interfacial Free Energy. *J. Chem. Phys.* **1958**, *28*, 258−267.
(49) Boltau, M.; Walheim, S.; Mlynek, J.; Krausch, G.; Steiner, U. Surface-Induced Structure Formation of Polymer Blends on Patterned Substrates. *Nature* **1998**, *391*, 877.
(50) Karim, A. Phase-Separation-Induced Surface Patterns in Thin Polymer Blend Films. *Macromolecules* **1998**, *31*, 857−862.
(51) Tanaka, H. Dynamic Interplay Between Phase Separation and Wetting in a Binary Mixture Confined in a One-Dimensional Capillary. *Phys. Rev. Lett.* **1993**, *70*, 53−56.
(52) Tanaka, K. Ultrathinning-Induced Surface Phase Separation of Polystyrene/Poly(vinyl methyl ether) Blend Film. *Macromolecules* **1995**, *28*, 934−938.
(53) Wang, H.; Composto, R. J. Understanding Morphology Evolution and Roughening in Phase-Separating Thin-film Polymer Blends. *Europhys. Lett.* **2000**, *50*, 622.
(54) Wang, H.; Composto, R. J. Kinetics of Surface and Interfacial Fluctuations in Phase Separating Polymer Blend Films. *Macromolecules* **2002**, *35*, 2799−2809.
(55) Briggs, D.; Seah, M. P. *Practical Surface Analysis by Auger and X-Ray Photoelectron Spectroscopy*; Wiley: New York, 1983; Appendix 4, p 1716.
(56) Composto, R. J.; Walters, R.M.; Genzer, J. Application of Ion Scattering Techniques to Characterize Polymer Surfaces and Interfaces. *Mater. Sci. Eng., R* **2002**, *38*, 107−180.
(57) Mayer, M. *Simnra User's Guide*; Max-Planck-Institute für Plasmaphysik: Garching, Germany, 1997.
(58) Cho, K.; Jeon, H. K.; Park, C. E.; Kim, J.; Kim, K. U. Plasma-Surface Modification of Biomaterials. *Polymer* **1996**, *37*, 143−206.
(59) Elemans, P. H. M.; Janssen, J. M. H.; Meijer, H. E. H. The Measurement of Interfacial Tension in Polymer/Polymer Systems : The Breaking Thread Method. *J. Rheol.* **1990**, *34*, 1311−1325.
(60) Wu, S. *Polymer Interface and Adhesion*; Marcel Dekker: New York, 1982; pp 420−447.
(61) Wu, S. Interfacial and Surface Tensions of Polymers. *J. Macromol. Sci., Polym. Rev.* **1974**, *10*, 1−73.
(62) Stokes, R. J.; Evans, D. F. *Fundamental of Interfacial Engineering*, 1st ed; Wiley-VCH: New York, 1997; pp 220−334.
(63) Geoghegan, M.; Krausch, G. Wetting at Polymer Surfaces and Interfaces. *Prog. Polym. Sci.* **2003**, *28*, 261−302.

(64) Sung, L. Phase Separation Kinetics and Morphology in a Polymer Blend with Diblock. Copolymer Additive. *J. Polym. Res.* **1996**, *3*, 139−150.
(65) Wang, H.; Composto, R. J. Wetting and Phase Separation in Polymer Blend Films: Identification of Four Thickness Regimes with Distinct Morphological Pathways. *Interface Sci.* **2003**, *11*, 237−248.
(66) Xue, L.; Han, Y. *Pattern,* Y. H. Pattern Formation by Dewetting of Polymer Thin Film. *Prog. Polym. Sci.* **2011**, *36*, 269−293.
(67) Liao, Y.; You, J.; Shi, T.; An, L.; Dutta, P. K. Phase Behavior and Dewetting for Polymer Blend Films Studied by In Situ AFM and XPS: From Thin to Ultrathin Films. *Langmuir* **2007**, *23*, 11107−11111.
(68) Wang, H.; Composto, R. J. Thin Film Polymer Blends Undergoing Phase Separation and Wetting: Identification of Early, Intermediate, and Late Stages. *J. Chem. Phys.* **2000**, *113*, 10386−10397.